Two-step Reactive Aid Sintering of $BaZr_{0.8}Y_{0.2}O_{3-\delta}$ Proton Conducting Ceramics

Siwei Wang[a], Yan Chen[b], Lingling Zhang [c], Cong Ren[a], Fanglin Chen[c,*], Kyle S. Brinkman[a,*]

[a] Department of Materials Science and Engineering, Clemson University, Clemson, SC, 29634, USA

[b] Chemical and Engineering Materials Division, Oak Ridge National Laboratory, Oak Ridge, Tennessee 37831, USA

c Department of Mechanical Engineering, University of South Carolina, Columbia, SC, 29208, USA

[*] Corresponding Author: Email: chenfa@cec.sc.edu; ksbrink@clemson.edu

Abstract

Ceramic-based proton conductors enable high temperature hydrogen economy applications such as hydrogen separation membranes, fuel cells, and steam electrolyzers. $BaZr_{0.8}Y_{0.2}O_{3-\delta}$ (BZY) proton conducting oxide possesses the highest level of proton conductivity reported to date, but the poor sinterability hinders its widespread utilization. In this paper, we report a two-step reactive aid sintering (TRAS) method involving the introduction of $BaCO_3$ and B_2O_3-Li_2O sintering aid for the preparation of dense BZY ceramics sintered at 1500^oC. The resulting BZY samples showed pure perovskite structure with more densified microstructure from 71.3% improved to 91.5%. The shrinkage during sintering was improved to 19.3% by

the TRAS method compared to 2.6% by conventional solid date reaction method. The bulk conductivity was improved due to the enhanced densification, while the grain boundary conductivity decreased due to the blocking behavior of the sintering aid, leading to a decrease in the total conductivity of the investigated proton conductor.

Key words: Proton Conductor, Solid Oxide Fuel Cells, Sinterability, Solid state reactive sintering, Sintering aid.

1. Introduction

Proton conducting oxides are a promising class of ceramic materials for energy conversion and storage applications such as proton conducting solid oxide fuel cells, high temperature hydrogen separation membranes, and steam electrolyzers [1-9]. There are two main types of perovskite oxides that are currently used for these applications: doped cerates and doped zirconates. The doped cerates such as rare earth doped $BaCeO_3$ and $SrCeO_3$ have demonstrated very high conductivity in humidified atmospheres as well as good sinterability. However, these materials possess poor thermodynamic stability towards water and CO_2, consequently their potential application is strictly limited [10]. On the contrary, doped $BaZrO_3$ is thermodynamically more stable than their cerate counterpart, which attracts more and more researchers' attention in recent years. However, the refractory nature of zirconium makes the $BaZrO_3$ based materials very difficult to densify, with a nominal sintering temperature of above 1700^oC, requiring a special high temperature furnace

and potentially leading to unfavorable evaporation of Ba from the A-site [11-12].

To overcome the drawback of poor sinterability, several methods aimed at improving sinterability, while maintaining the conductivity of doped $BaZrO_3$ have been attempted, such as adding sintering aids as well as utilization of new sintering methods. Haile's group has reported ZnO added BZY prepared by a wet-chemistry method [13]. The sintering temperature was reduced to 1300^{o}C with a surface grain size in the range of 1 μm. Irvine's group has also developed ZnO doped BZY by a solid state reaction method with a calcination temperature of 1400^{o}C and a final sintering temperature of 1325^{o}C [14-15]. CuO doped BZY was also densified at 1600^{o}C with an average grain size of 0.5-1μm [16]. Bi_2O_3 was also reported to improve the densification of BZY [17]. Here in this report, we introduce a B_2O_3-Li_2O as a liquid–phase sintering aid for BZY ceramic. Such sintering aid has been applied in dielectric and ferroelectric area [18-19]. The sintering temperature of $BaZr_{0.35}Ti_{0.65}O_3$ was lowered from 1500^{o}C to 1000^{o}C by introducing 4.75 wt% B_2O_3-Li_2O sintering aid [18]. However, the sintering aid should be carefully chosen taking into account to the overall defect chemistry of the BZY ionic conductivity system [20].

On the other hand, processing modifications such as the use of a reactive sintering method has been adopted to improve the densification as well as grain growth in BZY materials. The reactive sintering method is a recently development sintering method, where the reaction occurs during the sintering process, with some of the reactants (or

transition /secondary phases) functioning as sintering aids. Tong et al. introduced NiO directly into the oxide precursors of BZY to sinter dense ceramics, with the transition phase BaY_2NiO_5 functioning the un-intended rule as a sintering aid. Grain size as large as 5 μm was achieved after sintering at 1500^{o}C for 24 h.[8, 21] Chen, *et al.* further found that BaY_2NiO_5 was formed as a secondary phase after sintering, and transformed to Ni metallic particles after being treated in wet reducing atmosphere at high temperature.[7] This reactive sintering method has been verified by Ricote by obtaining BZY pellets with 1.3 μm grain size after sintering at 1500^{o}C for 4 h.[22] Haile's group developed a similar reactive sintering method without using sintering aid, but rather utilizing $BaCO_3$ as precursor.[23] The existence of $BaCO_3$ at a calcination temperature of 850^{o}C by sol-gel method is necessary to improve the sinterability of BZY, with which a grain size of 1.4 μm was obtained after remaining at 1600^{o}C for 24 h [23]. The conductivity was significant improved since no extra sintering aid was introduced; however this sintering temperature is still too high for most applications.

In this study, we introduced a Two-step Reactive Aid Sintering (TRAS) method to BZY ceramic sintering that combines the advantage of reactive sintering and the sintering aid methods. The sample is firstly sintered by reactive sintering strategy at an intermediate temperature, showing a relatively large grain size but still with porous microstructure. Subsequently, the sample is ground into powder and the B_2O_3-Li_2O (B-Li) sintering aid is added to enhance grain boundary diffusion through higher

diffusion coefficients in the local liquid phase present at the grain boundary. The obtained pellet samples are then sintered at 1500^{o}C, aiming at obtaining large grained and densified sample with a relatively low sintering temperature. The physicochemical properties of the samples were studied.

2. Experimental

2.1 Sample preparation methods

BZY samples, with nominal composition of $BaZr_{0.8}Y_{0.2}O_{2.9}$ were prepared by conventional solid state reaction (SSR) method and the sol-gel based combined EDTA-citric (CEC) sol-gel method, respectively. [24-25] For the conventional SSR method, stoichiometric amount of $BaCO_3$ (Alfa Aesar, 99.8%), ZrO_2 (Alfa Aesar, 99.7%) and Y_2O_3 (Alfa Aesar, 99.9%) were mixed together by ball-milling in ethanol for 24 h. After drying, the obtained powders were pressed into pellets, followed by calcining at 1100^{o}C for 10 h in air with a heating rate of 3^{o}C min^{-1}. The pellets were then ground into powders which were subsequently mixed with 5 wt% polyvinyl alcohol (PVA) binder and uniaxially pressed into pellets under a pressure of 400 MPa. The green pellets were sintered at 1500^{o}C for 10 h in air with a heating rate of 2 ^{o}C min^{-1}. For the samples prepared by CEC method, $Ba(NO_3)_2$ (Alfa Aesar, 99.95%), $ZrO(NO_3)_2 \cdot xH_2O$ (Alfa Aesar, 99.9%), $Y(NO_3)_3 \cdot 6H_2O$ (Alfa Aesar, 99.9%) were titrated and dissolved into solutions. Ethylenediaminetetraacetic acid (EDTA, Alfa Aesar, 99%) and citric acid (Alfa Aesar, 99%) were used as chelating and complexing agents, respectively. Ammonium hydroxide (Sigma-Aldrich, NH_3 content 28.0 to

30.0%) was added to promote the dissolution of EDTA in deionized water. The metal precursors were then stoichiometrically added into the chelating and complexing agents with the molar ratio metal nitrates: citric acid : EDTA = 1 : 1.5 : 1.2. The solution was stirred at room temperature for 24 h to achieve full complexation, followed by heat treatment in a kitchen microwave oven to assist in foaming. The dry foam was subsequently fired at 600^{o}C for 4 h in air to remove organic residue, resulting in light-colored powders. The powder was then calcined at 850^{o}C for 10 h in air with a heating rate of 3^{o}C min^{-1}. The obtained powder was pulverized and mixed with 5 wt% polyvinyl alcohol (PVA) binder and pressed uniaxially into pellets under 600 MPa. The green pellets were finally sintered at 1500^{o}C for 10 h in air with a heating rate of 2^{o}C min^{-1}.

The TRAS method was applied to both samples with BZY powders prepared from the SSR and CEC methods. The samples were sintered at 1500^{o}C by the reactive sintering strategy to obtain a relatively large grain size but retain a porous microstructure. The samples were subsequently ground into powders and the B_2O_3-Li_2O sintering aid was added and mixed into the powder to enhance the grain boundary diffusion. 1 wt% B_2O_3-Li_2O sintering aid was introduced to the as prepared BZY powders. The obtained pellet samples were then re-sintered at 1500 ^{o}C.

2.2 Characterizations

X-ray diffractometer (Rigaku, Japan) with graphite-monochromatized Cu Kα

radiation (λ- 1.5418 Å) was employed to record the X-ray diffraction patterns (XRD) of the samples. A scanning rate of 2^{o} min^{-1} was employed to characterize the phases of the samples while a slower scanning rate of 0.4^{o} min^{-1} was used to perform refinement of the XRD patterns. The diffraction patterns were analyzed by performing Rietveld refinement by General Structure Analysis System (GSAS) package and the graphical user interface (EXPGUI).[26-27] The microstructures of the sintered pellets were examined by a field emission scanning electron microscopy (FESEM, Zeiss Ultra). The relative density was measured by Archimedes method and the porosity was estimated by the ImageJ software. For conductivity measurements, the sintered pellets were polished and applied with platinum paste on both sides and then baked at 950^{o}C for 30 min to form the current collector. Platinum wires were attached to the surfaces of the Pt current collector. Electrical conductivity tests were conducted using a Zahner IM6 Electrochemical Workstation (ZAHNER-Electrik GmbH & Co., Kronach, Germany) in the frequency range from 0.1 Hz to 8 MHz at different testing environments. The conductivity measurement was carried out in dry air (dynamic air flowing through a silica gel and a $CaSO_4$ sand), wet air and wet H_2 (both containing 3vol% H_2O, obtained by flowing gases through a water bubbler at room temperature) at a temperature range of 400-700^{o}C. Thermal behaviors of the samples were characterized by a NETZSCH DIL 402C pushrod dilatometer from room temperature to 1500^{o}C with a heating rate of 3^{o}C min^{-1}.

3. Results and discussion

3.1. XRD analysis

Fig. 1 (a) shows the XRD patterns of the SSR sample calcined at 1100^{o}C, and CEC sample calcined at 850^{o}C, respectively. Trace amount of $BaCO_3$ and ZrO_2 can be detected besides the main BZY phase. As literature reported [23], the existence of $BaCO_3$ is necessary for the reactive sintering process. Fig. 1(b) shows the XRD spectra of the samples sintered at 1500^{o}C, as well as those sintered by TRAS method at 1500^{o}C for 10h. All the samples show pure perovskite structure without secondary phases. Further detailed analysis for the slow scanned XRD patterns of the BZY powders mixed with Si powder as an internal reference standard was conducted to determine the accurate peak positions for the XRD patterns. Rietveld refinement for the XRD patterns of the composites as shown in Fig. 2 confirmed the decrease of lattice parameter due to the introduction of the B-Li sintering aid and re-sintering. Detailed refined results are shown in Table I. The introduction of B-Li sintering aid does not introduce impurities on the XRD patterns as seen for the SSR_TRAS and the CEC_TRAS samples. At the meantime, the introduction of small B and Li ions into BZY will lead to shrinkage of the lattice. The possible evaporation of B-Li sintering aid during the sintering process will also result in a smaller amount of the B-Li sintering aid in the materials compared with the targeted compositions.

3.2. Microstructural analysis

As shown in Fig. 3 are the SEM images of the starting powders for (a) CEC sample, and (b) SSR sample. CEC sample shows porous foam like morphology coming from

the evaporation and buring of the precursor solution. In comparison, the SSR powder shows uniform distributed particles with paticle size of 0.2-0.5 μm. The different morphologies of the starting powders would resulted in different microstructure of the sintered samples. Fig. 4 shows the cross-sectional SEM pictures of the precursor pellets and the samples applied with the TRAS method, all sintered at 1500^{o}C for 10 h. It can be seen from Fig. 4(a) that the precursor SSR sample prepared by solid reactive sintering method at 1500^{o}C for 10 h shows a porous microstructure. The porosity is 23.3% measured from the SEM picture (See Fig. S1) with an average grain size of 0.82 μm, with the relative density of 71.3% measured by Archimedes' method. While for the sample sintered by the TRAS method at the same condition (1500^{o}C for 10 h), a fully densified microstructure was obtained as shown in Fig. 4(b) with an average grain size of round 1.03 μm and relative density of 91.5% from theoretical value. The CEC sample prepared by sol-gel method also shows loose microstructure similar to the sample prepared by the SSR method (porosity of 33.4%, see Fig. S2), but with smaller grain sizes, at around 0.30 μm (Fig. 4(c)) and a relative density of 81.5%. As shown in Fig. 4(d), the CEC sample prepared by TRAS method also exhibited a dense microstructure, with average grain size of around 0.45 μm and a relative density of 88.2%. It is clear that the B-Li sintering aid effectively improved the migration of the grain boundary during the second step sintering, leading to a densified microstructure as well as grown grain sizes, even though the maximum sintering temperature remained the same during the re-sintering process.

3.3 Sintering behaviors

Fig. 5 shows the sintering behaviors of the samples with different preconditions for the dilatometry measurement. It can be seen that for the precursor BZY sample prepared by the SSR method, the shrinkage is 8.5% up to 1550^{o}C (Black). While by applying 1 wt% B-Li sintering aid into the sintered precursor sample, a shrinkage rate of 19.3% is achieved (Red). The precursor BZY sample prepared by CEC method shows similar trend, with the precursor sample shrinking 13.9% (Green) and the TRAS sample shrinking 11.4%, a value slightly less than that of the precursor CEC sample (Blue). For comparison, the SSR sintered pellet was ground and pressed into pellet again for dilatometry measurement. A low shrinkage rate of 2.6% was obtained (which were caused by the burning out of the organic binders). This is expected as it can be treated as a re-sintering of the sintered sample (Magenta), which has little effect on improving the sintering behavior of the material. Considering the preconditions of the TRAS samples which are both pre-sintered at 1500^{o}C for 5h, the shrinkage rates obtained from the TRAS method are remarkable.

Besides the shrinkage ratio, from the shrinkage rate curves of the samples shown in Fig. 5 it is observed that the TRAS method facilitated the shrinkage of the samples to start densifying at a temperature of around 1000^{o}C and the maximum shrinkage rate was achieved at 1125^{o}C. Without applying the TRAS method, the shrinkage starts at ~1300^{o}C for CEC and at ~1500^{o}C for SSR sample. Lowering the densification temperature and achieving densified ceramics at lower temperature are the

contributions of the TRAS method.

3.4. Electrical properties

The electrical properties of the samples were obtained from the AC impedance spectra. Fig. 6 shows the typical Nyquist plots of CEC sample tested under dry air environment at different temperatures. The impedance spectra typically have three semi-circles corresponding to the bulk, grain boundary and electrode responses from high to low frequencies. Such three semicircles can be simulated by parallel R-CPE (constant phase element) equivalent circuit model. With an increase in the testing temperature, the semi-circle corresponding to the bulk conduction response gradually disappears. The bulk resistance is then derived from the high frequency intercept of the intermediate arc with the real axis (as shown in Fig. 6 inset).

Fig. 7 shows the total conductivity of the sintered samples in different atmospheres. It can be seen from Fig. 7(a) that the SSR sample shows a typical proton conducting behavior. At lower temperature regime (below 600^{o}C), the sample tested in wet H_2 has the highest conductivity and the lowest activation energy, while the sample tested in dry air possesses the highest activation energy. The proton conductivity was enhanced by the introduction of H_2 and water. The proton concentration decreases with an increase in temperature, caused by the dehydration of the materials due to the exothermic nature of the Kröger-Vink reaction

$$H_2O_{(g)} + O_O^{\times} + V_O^{\bullet\bullet} = 2OH_O^{\bullet} \qquad (1)$$

Where $O_O^{\times}$ means nutral oxygen sites, $V_O^{\bullet\bullet}$ oxygen vacancy, and $OH_O^{\bullet}$ indicates

proton charge carrier formed within the structure by attaching to the lattice oxygen. Such dehydration behavior resulted in a decreased activation energy at high temperatures in wet H_2, showing a bowed shape for the conductivity curve. Such decrease in the activation energy can also be observed in the CEC sample as shown in Fig. 7(c). However, this curvature behavior is not clear in the TRAS samples, e generally are higher than their counterparts, indicating the introduction of B-Li sintering aid leads to this higher activation energy due to the insulating nature towards ionic defect transport. The conductivity values are approximately one order of magnitude lower than the values without the sintering aid. Detailed results are shown in Table II.

The bulk and grain boundary conductivity are separated and presented in Fig. 8. For the bulk conduction, the activation energies are from 0.48-0.61 eV, which are characteristic of ionic conduction. For the CEC_TRAS samples, improved bulk conductivity was achieved at the entire testing temperature range. For the SSR_TRAS sample, improved conductivity can be observed at temperatures higher than 500^{o}C due to the higher activation energy of the sample. The improved bulk conductivity is due to the improved densification conditions of the TRAS samples in which the densified microstructure with larger grains exhibits a higher proportion of bulk conductivity. Assuming that B and/or Li ions are incorporated into the B site of the perovskite structure (with the Shannon ionic radii of the B-site cations, r_{Zr}=0.72 Å, r_B=0.27 Å, r_{Li}=0.76 Å, respectively [28]), increased vacancy concentrations on both

Ba and oxygen sites are expected which will in turn improve the ionic conductivity [13]:

$$B_2O_3 \xrightarrow{BaZrO_3} 2B_{Zr}^{'} + 3O_O^{\times} + 2V_{Ba}^{''} + 3V_O^{\bullet\bullet} \qquad (2\text{-}1)$$

which means the introduction of B_2O_3 introduced oxygen vacancy and barium non-stoichiometry, or

$$2BaO + B_2O_3 \xrightarrow{BaZrO_3} 2B_{Zr}^{'} + 5O_O^{\times} + 2Ba_{Ba}^{\times} + V_O^{\bullet\bullet} \qquad (2\text{-}2)$$

which suggests that the doping of B_2O_3 consumes BaO in the compound. A similar situation may happen with the introduction of Li_2O:

$$Li_2O \xrightarrow{BaZrO_3} 2Li_{Zr}^{'''} + O_O^{\times} + 2V_{Ba}^{''} + 5V_O^{\bullet\bullet} \qquad (3\text{-}1)$$

or

$$2BaO + B_2O_3 \xrightarrow{BaZrO_3} 2B_{Zr}^{'} + 5O_O^{\times} + 2Ba_{Ba}^{\times} + V_O^{\bullet\bullet} \qquad (3\text{-}2)$$

Consistent with the XRD result, the introduction of B-Li sintering aid led to shrinkage of the lattice structure. Regarding the likely defect mechanism, equation (2) would be the simplest situation resulting in only that only Boron ions doped into the B-sites. The situation described in equation (3) would not happen alone since the ionic radius of Li^+ is larger than Zr^{4+} with a coordination number of 6 based on Shannon radii.[28] However, equation (3) may happen together with equation (2), with the combined effect of decreasing the lattice parameter. There is also the possibility that the B and/or Li ions may be doped into the interstitials of the BZY structure.

Differences also exist in the grain boundary conductivity as a function of processing conditions. The grain boundary conductivity of the SSR and CEC samples are

generally 1 order of magnitude higher than their TRAS counterparts. The activation energy values are also lower, with ~1 and 1.3 eV for SSR and CEC samples respectively. This result is consistent with observations that the sintering aid improved the grain boundary migration during the sintering process, while at that same time contributed to the reduction in grain boundary conductivity due to the insulating nature of the sintering aid. It is also of note that the SSR samples displayed higher grain boundary conductivity than the CEC samples, for both the conventional and TRAS methods, indicating that the larger grains are beneficial for the grain boundary conduction.

For our TRAS sample, the bulk conductivity is among the highest level reported in this material system (10^{-3} S cm^{-1} at 500^{o}C), which is due to the large grained, dense microstructures of the sample. However, the grain boundary conductivity is approximately 1 order of magnitude lower than the bulk conductivity (and 1-3 orders lower than the literature results), which reduces the total conductivity. Consequently, the B-Li sintering aid is believed to be segregated at the grain boundaries, so that the ionic conduction was blocked by a grain boundary impurity phase. Although the grain boundary impurity phase improved the sinterability of the ceramics, and thus enhanced the bulk conduction, the sintering aid also exhibited a blocking effect that lowered the grain boundary conductivity. The combined effect resulted in lowered total conductivity.

4. Conclusions

Densified BZY samples were successfully prepared by a two-step reactive aid sintering method with the B-Li sintering aid. The first reactive sintering step at 1500^{o}C introduced $BaCO_3$ and the sample reached a density of ~70%. The introduction of B_2O_3-Li_2O sintering aid during the second sintering step at 1500^{o}C produced fully densified BZY ceramics. The structure remained pure phase with a reduced lattice parameter due to the introduction of the B-Li sintering aid. The bulk conductivity was improved due to the densified microstructure with large grains, which are among the highest level reported in this material system. The TRAS method is thus a promising way to produce dense, large grained ceramic oxides due to its simplicity and effectiveness. However, investigation of the optimized composition, concentration and mechanism of incorporation of the B-Li sintering aid is needed in order to balance the densification of the sample and the deterioration of the grain boundary conductivity.

ACKNOWLEDGMENT

We gratefully acknowledge the financial support from the SCUREF/SRNS/DOE under award # B139006. Y. Chen thanks the support from Materials, Science and Engineering Division, Office of Basic Energy, Sciences, Office of Science, U.S. Department of Energy. K. Brinkman acknowledges the Energy Frontier Research Center on Science Based Nano-Structure Design and Synthesis of Heterogeneous Functional Materials for Energy Systems (HeteroFoaM Center) funded by the U.S.

Department of Energy, Office of Science, Office of Basic Energy Sciences (Award no. DE-SC0001061). K. Brinkman also wishes to acknowledge a 2014 Clemson TIGER Grant on Materials and Processes for Natural Gas Utilization.

References

1. H. Iwahara, T. Esaka, H. Uchida and N. Maeda, *Solid State Ionics* 3-4, 359 (1981).
2. K. D. Kreuer, *Annu. Rev. Mater. Res.* 33, 333 (2003).
3. L. Yang, S. Z. Wang, K. Blinn, M. F. Liu, Z. Liu, Z. Cheng and M. L. Liu, *Science* 326, 126 (2009).
4. E. Fabbri, L. Bi, H. Tanaka, D. Pergolesi and E. Traversa, *Adv. Funct. Mater.* 21, 158 (2011).
5. S. Wang, L. Zhang, L. Zhang, K. Brinkman and F. Chen, *Electrochim. Acta* 87, 194 (2013).
6. S. Wang, Y. Chen, S. Fang, L. Zhang, M. Tang, K. An, K. S. Brinkman and F. Chen, *Chem. Mater.* 26, 2021 (2014).
7. S. Fang, S. Wang, K. S. Brinkman and F. Chen, *J. Mater. Chem. A* 2, 5825 (2014).
8. J. Tong, D. Clark, L. Bernau, M. Sanders and R. O'Hayre, *J. Mater. Chem.* 20, 6333 (2010).
9. S. Wang, L. Zhang, Z. Yang, L. Zhang, S. Fang, K. Brinkman and F. Chen, *J. Power Sources* 215, 221 (2012).
10. S. Wang, F. Zhao, L. Zhang, K. Brinkman and F. Chen, *J. Alloys Compd.* 506, 263 (2010).
11. C. D. Savaniu, J. Canales-Vazquez and J. T. S. Irvine, *J. Mater. Chem.* 15, 598 (2005).
12. S. Wang, Y. Liu, J. He, F. Chen and K. S. Brinkman, *Int. J. Hydrogen Energy* 40, 5707.
13. P. Babilo and S. M. Haile, *J. Am. Ceram. Soc.* 88, 2362 (2005).
14. S. W. Tao and J. T. S. Irvine, *Adv. Mater.* 18, 1581 (2006).
15. S. Tao and J. T. S. Irvine, *J. Solid State Chem.* 180, 3493 (2007).
16. D. Gao and R. Guo, *J. Alloys Compd.* 493, 288 (2010).
17. S. Le, J. Zhang, X. Zhu, J. Zhai and K. Sun, *J. Power Sources* 232, 219 (2013).
18. X. Chou, J. Zhai, J. Sun and X. Yao, *Ceram. Int.* 34, 911 (2008).
19. S. Wang, J. Zhai, X. Chou and X. Yao, *J. Funct. Mater.* 40, 767 (2009).
20. Z. Sun, E. Fabbri, L. Bi and E. Traversa, *Phys. Chem. Chem. Phys.* 13, 7692 (2011).
21. J. Tong, D. Clark, M. Hoban and R. O'Hayre, *Solid State Ionics* 181, 496 (2010).
22. S. Ricote, N. Bonanos, A. Manerbino and W. G. Coors, *Int. J. Hydrogen Energy* 37, 7954 (2012).
23. Y. Yamazaki, R. Hernandez-Sanchez and S. M. Haile, *Chem. Mater.* 21, 2755 (2009).
24. S. Wang, F. Zhao, L. Zhang, K. Brinkman and F. Chen, *J. Power Sources* 196, 7917 (2011).
25. L. Zhang, Z. Mao, J. D. Thomason, S. Wang and K. Huang, *J. Am. Ceram. Soc.* 95, 1832

(2012).
26. A. C. Laurson, Von Dreele, R.B.: *General Structure Analysis System (GSAS)*. (Los Alamos National Laboratory Report, 2000).
27. B. Toby, *J. Appl. Crystallogr.* 34, 210 (2001).
28. *http://abulafia.mt.ic.ac.uk/shannon/ptable.php*.
29. R. B. Cervera, Y. Oyama, S. Miyoshi, K. Kobayashi, T. Yagi and S. Yamaguchi, *Solid State Ionics* 179, 236 (2008).

Table I. Structural parameters for the samples by XRD diffraction fitted by Rietveld refinement.

Parameters	**CEC**	**SSR**	**CEC_TRAS**	**SSR_TRAS**
a (Å)	4.2043(8)	4.20009(9)	4.19851(6)	4.1990(1)
R_{wp}	0.1402	0.1078	0.1170	0.1258
R_p	0.0926	0.0813	0.0906	0.1013
χ^2	3.732	3.153	2.655	2.261

Table II. Sinterability, conductivity values (at 500^{o}C) and Activation Energy values of BZY samples.

Sample	**Sintering Condition**	**Grain Size (μm)**	**Total (S cm^{-1})**	**Bulk (S cm^{-1})**	**Grain Boundary (S cm^{-1})**	**Atmos.**	**Ea (eV)**	**Ref.**
BZY20-SSR	1500^{o}C, 10 h, oxides	1	1.4×10^{-4}	2.1×10^{-3}	1.5×10^{-4}	Dry air	0.96	This work
BZY20-B-Li	1500^{o}C, 10 h, oxides	1	1.1×10^{-5}	2.4×10^{-3}	1.1×10^{-5}	Dry air	1.29	This work
BZY20-CEC	1500^{o}C, 10 h, nitrates	0.35	7.8×10^{-5}	2.1×10^{-3}	8.1×10^{-5}	Dry air	1.07	This work
BZY20-B-Li	1500^{o}C, 10 h, nitrates	0.35	7.7×10^{-6}	4.1×10^{-3}	7.7×10^{-6}	Dry air	1.3	This work
BZY20-ZnO	1325^{o}C, 10 h,	-	4.8×10^{-4}	7.6×10^{-4}	1.5×10^{-3}	Wet 5% H_2/Ar	0.23	Irvine[15]
BZY20-Li	1600^{o}C, 6 h, wet chemistry nitrates	0.43	2.7×10^{-3}	3.5×10^{-3} (350oC)	7.4×10^{-4} (350oC)	Wet 10% H_2/Ar	0.48	Traversa [20]
BZY20	1600^{o}C, 24 h Reactive sintering, nitrates	1	2.2×10^{-2}	1.2×10^{-2} (350oC)	1.0×10^{-2} (350oC)	wet N_2 or Ar	-	Haile [23]
BZY20	1500^{o}C, 20 h, alkoxides	0.2	4×10^{-3}	-	-	Wet Ar	0.54	Cervera [29]

Figure Captions

Fig. 1 XRD patterns of BZY samples **(a)** calcined precursor samples, **(b)** The samples sintered at 1500^{o}C. CEC_TRAS: sample prepared by CEC method and re-sintered by TRAS method with the introduction of B-Li sintering aid, SSR_TRAS: sample prepared by SSR method and re-sintered by TRAS method with the introduction of B-Li sintering aid.

Fig. 2 Rietveld refinement result for the XRD patterns of samples mixed with Si employed as internal reference standard, : **(a)** SSR sample pellet as prepared, **(b)** SSR sample prepared by TRAS method, **(c)** CEC sample pellets as prepared, **(d)** CEC sample prepared by TRAS method.

Fig. 3 Cross-sectional SEM pictures of sample pellets sintered at 1500^{o}C for 10h: **(a)** SSR sample pellet as prepared, **(b)** SSR sample prepared by TRAS method, **(c)** CEC sample pellets as prepared, **(d)** CEC sample prepared by TRAS method.

Fig.4 Sintering behaviors of the samples prepared via different procedures. Black: SSR sample precalcined at 1100^{o}C, Red: SSR_TRAS sample pre-sintered at 1500^{o}C, with 1 wt% B-Li sintering aid added, Green: CEC sample precalcined at 850^{o}C; Blue: CEC_TRAS sample pre-sintered at 1500^{o}C, with 1wt% B-Li sintering aid added; Magenta: SSR sintered pellet, ground, and pressed into pellet again for dilatometry measurement.

Fig. 5 Typical Nyquist Plots of CEC sample tested in dry air.

Fig. 6 Total conductivity of the sintered samples in different atmospheres.

Fig. 7 The Bulk and Grain Boundary (GB) conductivity of the samples tested in dry air.

Fig.1

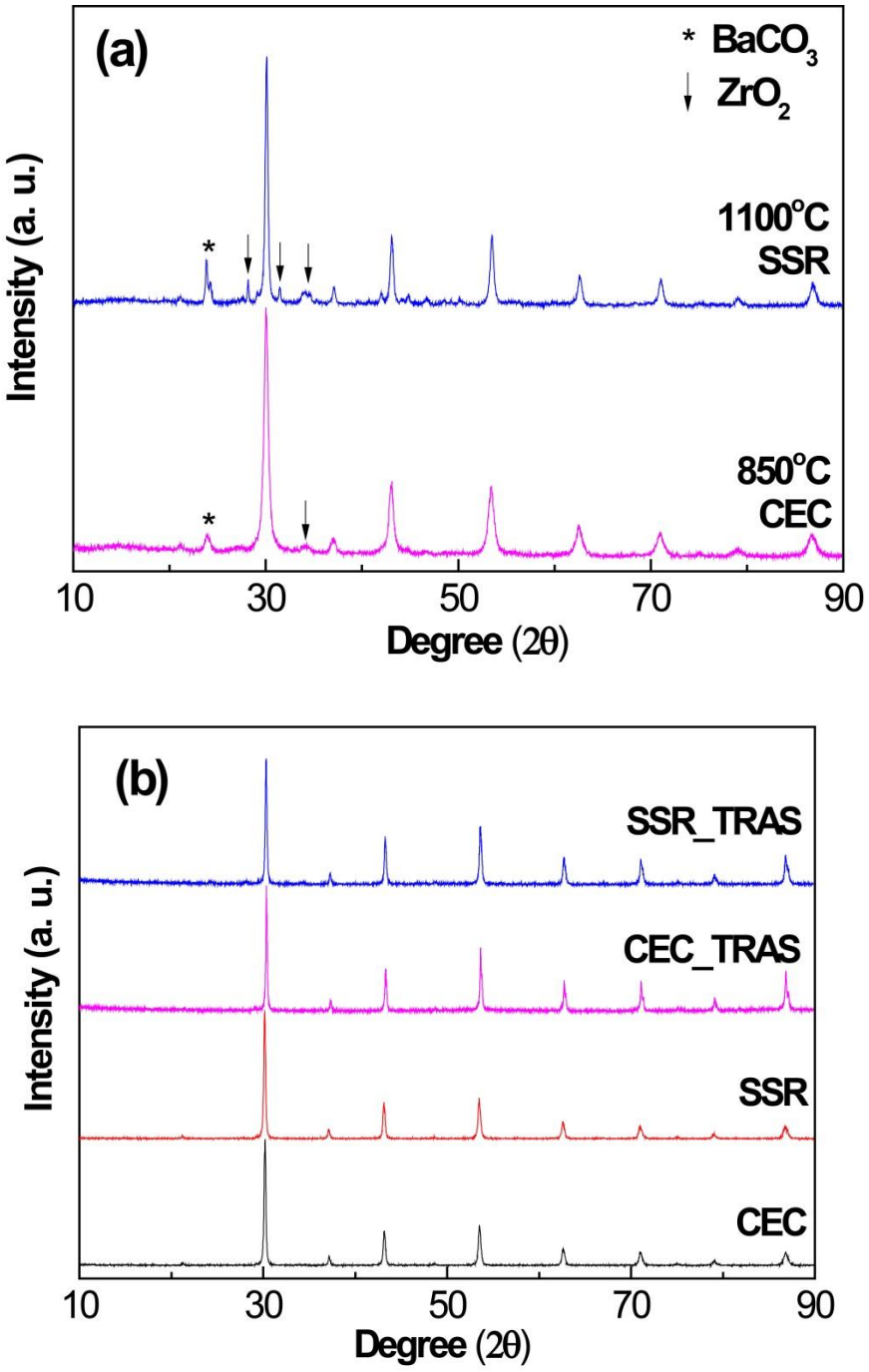
(a)
* BaCO3
ZrO2
1100°C
SSR
850°C
CEC
Intensity (a. u.)
10
30
50
70
90
Degree (2θ)
(b)
SSR_TRAS
CEC_TRAS
SSR
CEC
Intensity (a. u.)
10
30
50
70
90
Degree (2θ)

Fig. 2

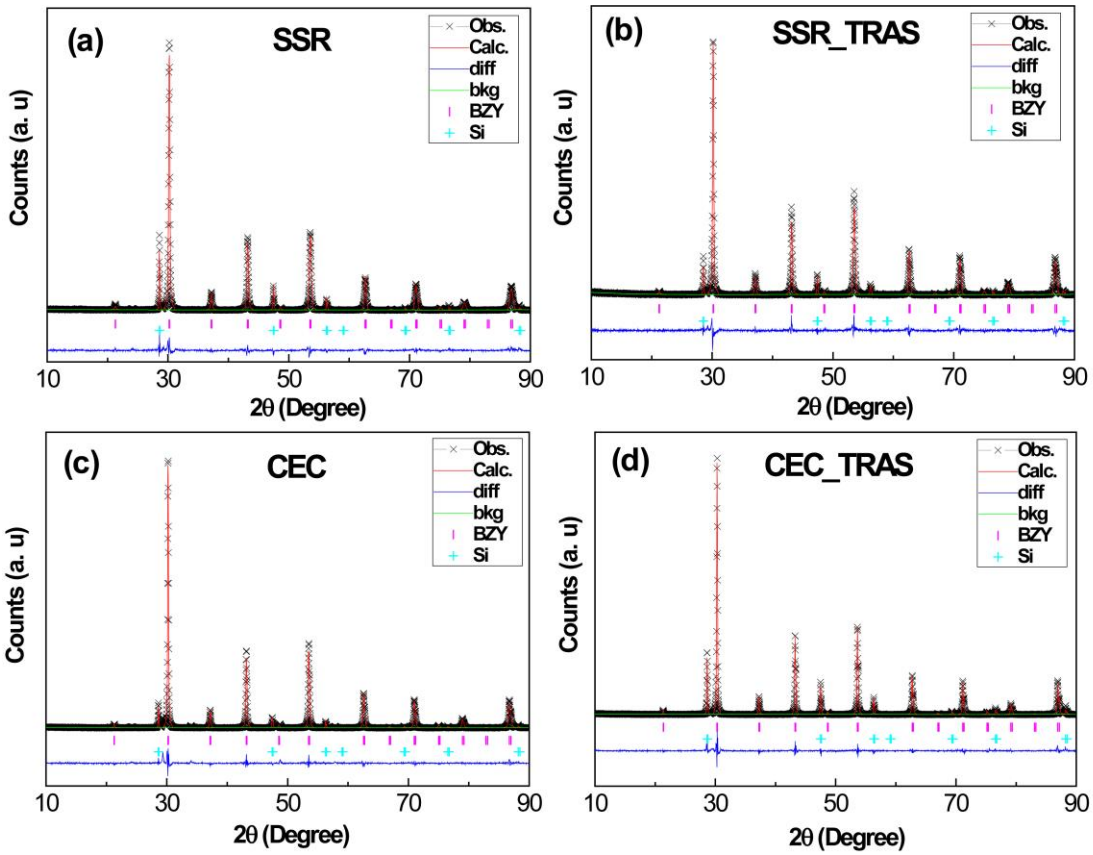

Fig. 2 Rietveld refinement result for the XRD patterns of samples mixed with Si employed as internal reference standard, : **(a)** SSR sample pellet as prepared, **(b)** SSR sample prepared by TRAS method, **(c)** CEC sample pellets as prepared, **(d)** CEC sample prepared by TRAS method.

Fig. 3

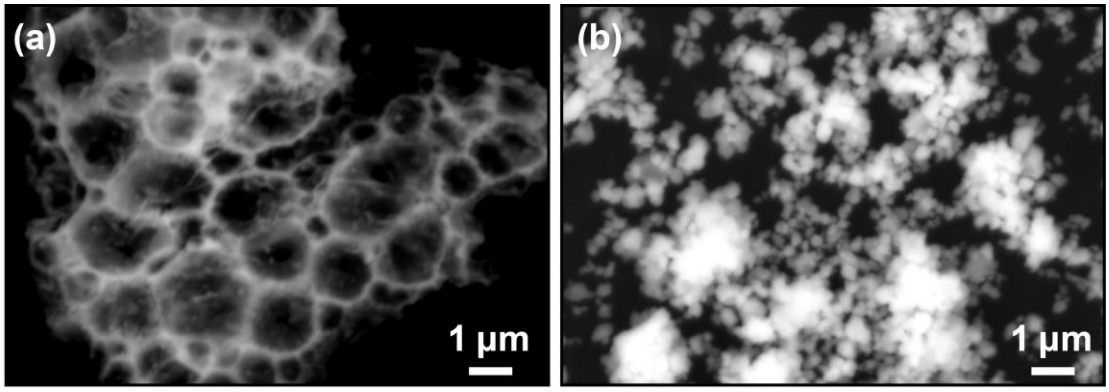

Fig. 3 SEM images of sample powders for (a) CEC sample powder heated at 850^{o}C, (b) SSR sample calcined at 1100 ^{o}C.

Fig. 4

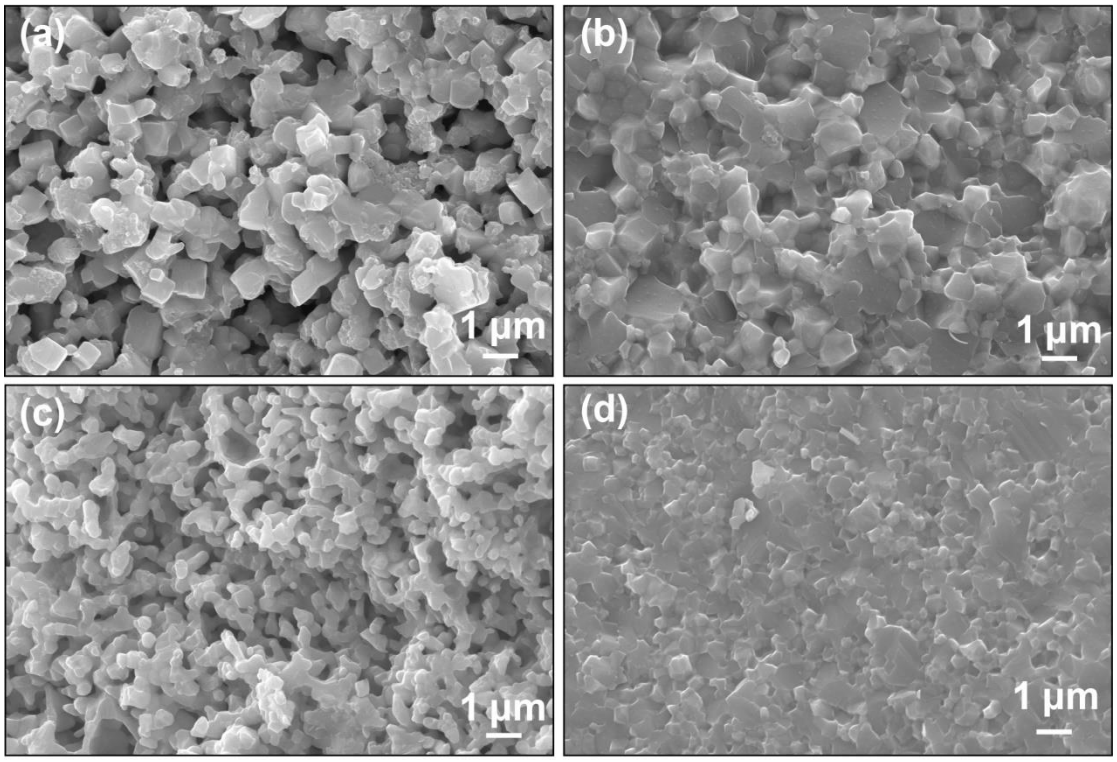

Fig. 4 Cross-sectional SEM pictures of sample pellets sintered at 1500^{o}C for 10h: **(a)** SSR sample pellet as prepared, **(b)** SSR sample prepared by TRAS method, **(c)** CEC sample pellets as prepared, **(d)** CEC sample prepared by TRAS method.

Fig. 5

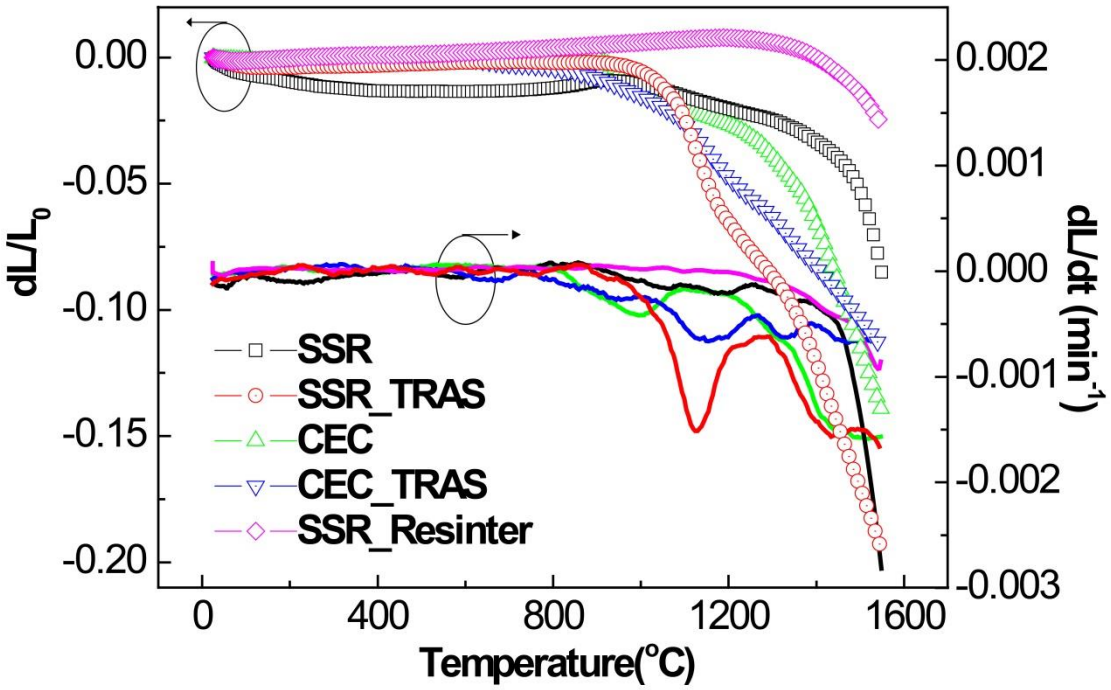

Fig. 5 Sintering behaviors of the samples prepared via different procedures. Black: SSR sample precalcined at 1100°C, Red: SSR_TRAS sample pre-sintered at 1500°C, with 1 wt% B-Li sintering aid added, Green: CEC sample precalcined at 850°C; Blue: CEC_TRAS sample pre-sintered at 1500°C, with 1wt% B-Li sintering aid added; Magenta: SSR sintered pellet, ground, and pressed into pellet again for dilatometry measurement.

Fig. 6

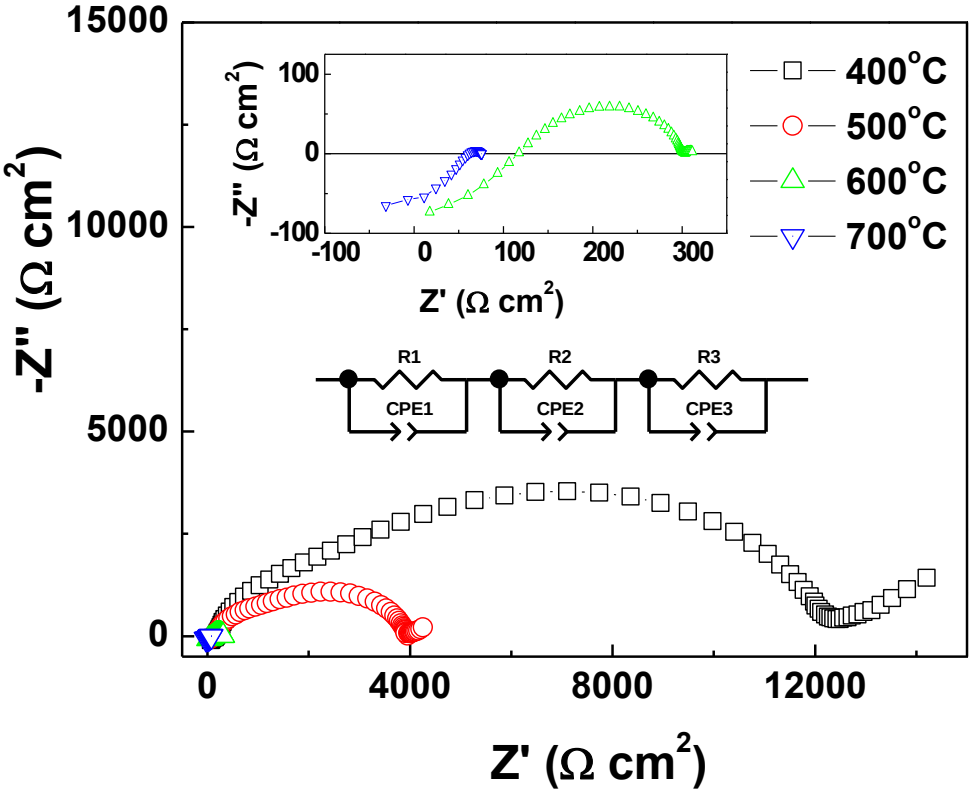

Fig. 6 Typical Nyquist Plots of CEC sample tested in dry air.

Fig. 7

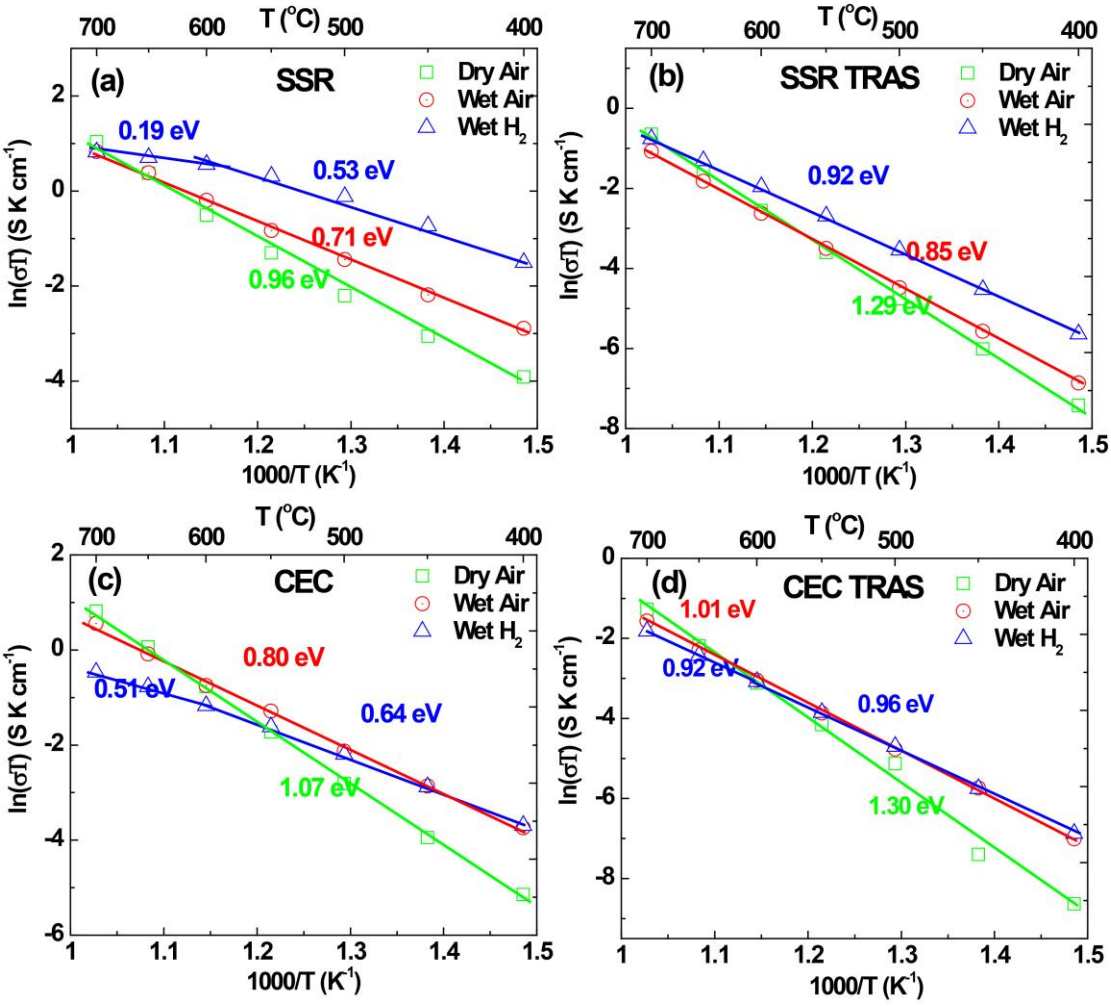

Fig. 7 Total conductivity of the sintered samples in different atmospheres.

Fig. 8

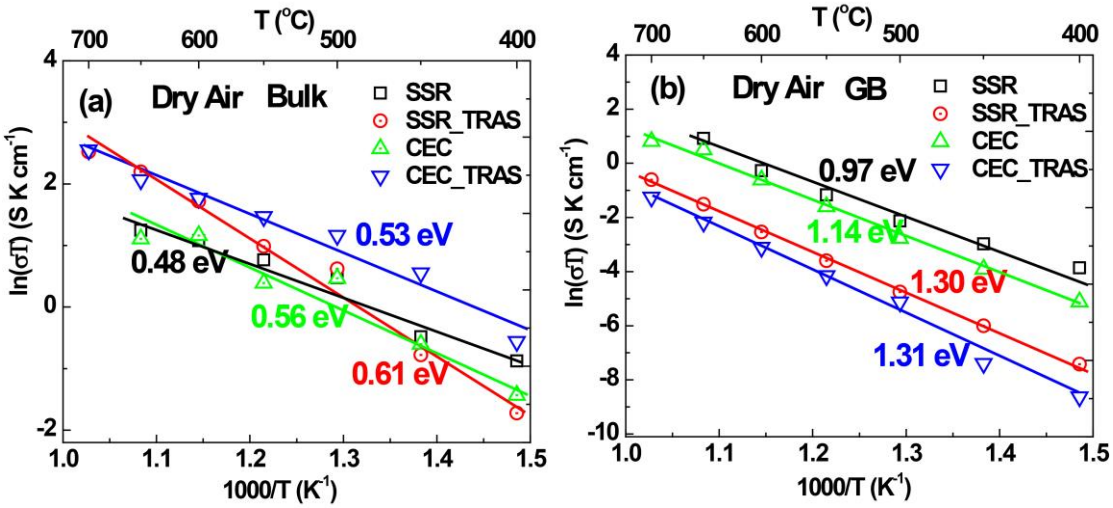

Fig. 8 The Bulk and Grain Boundary (GB) conductivity of the samples tested in dry air.